Z. C. Feng
B. He

Department of Mechanical and Aerospace Engineering, University of Missouri–Columbia, Columbia, MO 65211

S. J. Lombardo
Department of Chemical Engineering, University of Missouri–Columbia, Columbia, MO 65211

Stress Distribution in Porous Ceramic Bodies During Binder Burnout

A model has been developed for describing the stresses that arise during binder burnout in three-dimensional porous bodies. The pressure gradient that arises from the decomposition of binder in the pore space is treated as an equivalent body force. For input into the mechanics model, the pressure distribution is obtained from the analytical solution for three-dimensional porous bodies with anisotropic permeability. The normal and shear stresses are then calculated from finite element analysis for bodies of parallelepiped geometry. In general, the normal stresses occur at the center of the body and are an order of magnitude larger than the shear stresses. Both the normal and shear stresses depend on the body size, the body geometry, and on the permeability. [DOI: 10.1115/1.1460908]

1 Introduction

In the fabrication of ceramic components by powder processing routes, the strength of formed bodies is often enhanced by the addition of polymeric binders ([1]). These polymers are then removed in later processing steps by decomposing them at elevated temperature into gas-phase products. Two types of models ([2–20]) have appeared for describing how the degradation products exit the body. For bodies having large volume fractions of binder and thus low initial porosity, diffusion of the decomposition products through the remaining binder in the nearly filled space has been treated as the rate-limiting step ([2–11]). For bodies prepared with lower volume fractions of binder, gas-phase flow is the faster transport mechanism ([12–20]). In both cases, however, a distribution of pressure arises within the pore space of the body.

Depending on the processing parameters and the size of the component, the pressure increase inside the ceramic body during binder burnout can be so large as to decrease the product yield ([7,19,21]). In Liau et al. [19], it was demonstrated that the yield depended on the heating cycle and on the dimensions of square-parallelepiped multilayer ceramic capacitors (MLCs). The authors also noted that the flow of the gas-phase decomposition products in the MLCs was enhanced in the direction parallel to the planes containing the metal electrodes, which suggests that the permeability is anisotropic within the body. To describe these observations, an analytical model ([20]) has been developed for describing the pressure distribution during binder burnout in three-dimensional porous ceramic bodies with anisotropic permeability.

Although the pressure is known to increase within the body during binder burnout, the mechanical stresses arising during this process are ultimately what cause the ceramic component to fail. When the pressure distribution is known, the distribution of stresses can be calculated by adopting mechanical models for the ceramic body. Stangle and Aksay [14] used the stress formulation developed for partially saturated granular media ([22]) to calculate the stress distribution in spherical bodies. They considered both capillary stresses due to liquid-phase binders and stresses due to the increase in pressure arising from binder degradation products. Tsai [15] considered binder burnout in axisymmetric porous bodies. Both the radial and tangential stresses, which satisfy the equilibrium equations, were considered to consist of contributions from the gas phase and the solid phase (skeleton) by an equal amount. An isotropic constitutive law was used for the stress-strain relationship for the skeleton and the void fraction does not appear explicitly in the stress formulation. This pair of models take as their starting point that the local pressure and the local stress are linearly additive quantities.

In this paper, we propose a general three-dimensional model for the stresses caused by the buildup of internal pressure in a ceramic body during binder removal. Instead of calculating average stresses in porous media as is conventionally done ([23]), we model the ceramic body as a solid skeleton permeated by a gaseous phase whose pressure follows a known distribution. We first derive the equilibrium equations for the stresses on the skeleton and use an isotropic constitutive law. The gradient of the internal gas pressure is shown to be responsible for the stresses, and we develop a model formulation in which the pressure gradient is treated as an ''equivalent body force.'' Numerical methods are then used to solve for the stress distribution in rectangular parallelepipeds, a common geometry of ceramic capacitors.

2 The Mechanics Model

We make the following assumptions in the development of the model:

- The porous ceramic during the burnout process consists of a void fraction, ε, and a solid skeleton fraction, 1-ε.
- The void space is occupied by gas of internal pressure, p, which varies continuously in the pore space of the body. The gas phase cannot support shear stresses and both viscous and inertial stresses accompanying fluid flow are neglected.
- The solid skeleton can be modeled as an isotropic linear-elastic solid.

In Fig. 1, we show a free-body diagram of a two-dimensional infinitesimal volume. Force and moment equilibrium leads to the following equations:

$$(1-\varepsilon)\left(\frac{\partial \sigma_{xx}}{\partial x}+\frac{\partial \sigma_{xy}}{\partial y}\right)=\varepsilon\frac{\partial p}{\partial x} \tag{1}$$

$$(1-\varepsilon)\left(\frac{\partial \sigma_{xy}}{\partial x}+\frac{\partial \sigma_{yy}}{\partial y}\right)=\varepsilon\frac{\partial p}{\partial y} \tag{2}$$

where σ_{xx}, σ_{xy}, and σ_{yy} are the components of true stress on the skeleton. Obviously, an increase in internal pressure causes stress, an effect that is proportional to the void fraction, ε, appearing on the right-hand side of Eqs. (1) and (2). The factor of 1-ε on the

Contributed by the Applied Mechanics Division of THE AMERICAN SOCIETY OF MECHANICAL ENGINEERS for publication in the ASME JOURNAL OF APPLIED MECHANICS. Manuscript received by the ASME Applied Mechanics Division, Feb. 19, 2001; final revision, Oct. 16, 2001. Associate Editor: H. Gao. Discussion on the paper should be addressed to the Editor, Prof. Lewis T. Wheeler, Department of Mechanical Engineering, University of Houston, Houston, TX 77204-4792, and will be accepted until four months after final publication of the paper itself in the ASME JOURNAL OF APPLIED MECHANICS.

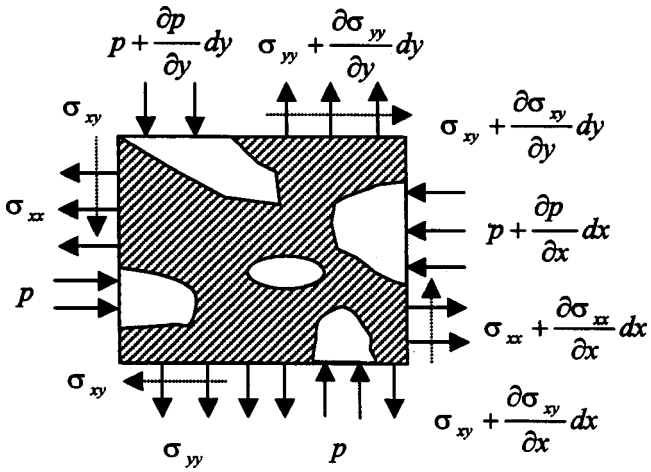

Fig. 1 Free-body diagram of an infinitesimal two-dimensional element showing the solid skeleton (hatched) and the continuous porous network. The shear stresses are denoted by the dashed arrows.

left-hand side of Eqs. (1) and (2) arises because only the skeletal part of the body bears the stress. The occurrence of a pressure gradient is thus equivalent to a body force throughout the continuum.

The stresses are often defined as the force per unit area without subtracting the nonload bearing voids. These nominal stresses, $\tilde{\sigma}$, are smaller than the true stresses as given by

$$\tilde{\sigma}_{ij}=(1-\varepsilon)\sigma_{ij} \tag{3}$$

where i and j correspond to x and y. In terms of the nominal stresses, the equilibrium equations become

$$\frac{\partial \tilde{\sigma}_{xx}}{\partial x}+\frac{\partial \tilde{\sigma}_{xy}}{\partial y}=\varepsilon\frac{\partial p}{\partial x} \tag{4}$$

$$\frac{\partial \tilde{\sigma}_{xy}}{\partial x}+\frac{\partial \tilde{\sigma}_{yy}}{\partial y}=\varepsilon\frac{\partial p}{\partial y}. \tag{5}$$

Note that the nominal stresses differ from the true stresses by a constant factor, which is only dependent on the void fraction.

The equilibrium equations in two dimensions can be generalized into three dimensions as

$$\frac{\partial \tilde{\sigma}_{xx}}{\partial x}+\frac{\partial \tilde{\sigma}_{xy}}{\partial y}+\frac{\partial \tilde{\sigma}_{xz}}{\partial z}=\varepsilon\frac{\partial p}{\partial x} \tag{6}$$

$$\frac{\partial \tilde{\sigma}_{xy}}{\partial x}+\frac{\partial \tilde{\sigma}_{yy}}{\partial y}+\frac{\partial \tilde{\sigma}_{yz}}{\partial z}=\varepsilon\frac{\partial p}{\partial y} \tag{7}$$

$$\frac{\partial \tilde{\sigma}_{xz}}{\partial x}+\frac{\partial \tilde{\sigma}_{yz}}{\partial y}+\frac{\partial \tilde{\sigma}_{zz}}{\partial z}=\varepsilon\frac{\partial p}{\partial z}. \tag{8}$$

To complete the description of the problem, the skeleton is assumed to follow isotropic elastic constitutive laws ([24]) with Young's modulus, E, and the Poisson's ratio, ν. An alternative approach ([25]) leading to the identical model is to use the theory of interacting continua as proposed by Green and Naghdi [26] and applied by Ortiz [27].

The relationship between the internal pressure and stress distributions described by Eqs. (6)–(8) can be clarified for the following special case. We consider two-dimensional problems (plane stress or plane strain) with body forces derivable from the gradient of a potential, which is the pressure in our case. The Airy stress function, Φ, can then be invoked by letting ([24]):

$$\tilde{\sigma}_{xx}=\varepsilon p+\frac{\partial^2\Phi}{\partial y^2},\quad \tilde{\sigma}_{xy}=-\frac{\partial^2\Phi}{\partial x\partial y},\quad \tilde{\sigma}_{yy}=\varepsilon p+\frac{\partial^2\Phi}{\partial x^2}. \tag{9}$$

The Airy stress function is then determined from solution to the nonhomogeneous biharmonic equation

$$\frac{\partial^4\Phi}{\partial x^4}+2\frac{\partial^4\Phi}{\partial x^2\partial y^2}+\frac{\partial^4\Phi}{\partial y^4}=D\left(\frac{\partial^2 p}{\partial x^2}+\frac{\partial^2 p}{\partial y^2}\right) \tag{10}$$

where the constant D depends on whether the problem is plane stress or plane strain. The plane-stress and plane-strain results can be generalized to sheet-like geometries (length in one direction is much smaller than the other two) or rod-like geometries (length in one direction is much larger than the other). Although numerical methods are required even to solve for Φ with these geometries, great simplification for two-dimensional problems can be achieved if the internal pressure satisfies the Laplace equation. Under these circumstances, the right-hand side of Eq. (10) becomes zero, and the biharmonic equation is thus homogeneous. If we further assume that no external loads are applied on the ceramic body, $\Phi=0$ is a solution which satisfies both the biharmonic equation and the boundary conditions. By uniqueness, we conclude that $\Phi=0$ everywhere within the body and thus the stresses inside the body are isotropic tensors and are proportional to the internal pressure as given by Eq. (9). This conclusion only holds for the two-dimensional case. In summary, stresses and internal pressures are related through differential equations; only in rare circumstances are they related by simple algebraic relations.

3 Stresses in Rectangular Parallelepipeds

To calculate the stresses in a three-dimensional ceramic body, we first need to know how the internal pressure varies with position. The starting point is to use Darcy's law for flow in porous media ([28]) when a source term is present. Applying conservation of mass then leads to a partial differential equation, the solution ([20]) to which describes the pressure distribution in a parallelepiped of dimensions L_x, L_y, and L_z, as

$$p=P_0\sqrt{1+\sum_{i=1,3,5,\ldots}\sum_{j=1,3,5,\ldots}\sum_{k=1,3,5,\ldots}A_{ijk}\cos\left(\frac{i\pi x}{L_x}\right)\cos\left(\frac{j\pi y}{L_y}\right)\cos\left(\frac{k\pi z}{L_z}\right)} \tag{11}$$

for $-L_x/2<x<L_x/2$, $-L_y/2<y<L_y/2$, $-L_z/2<z<L_z/2$, where P_0 is the ambient pressure surrounding the porous body, and

$$A_{ijk}=8C\left(\frac{2}{\pi}\right)^5\frac{1}{ijk[i^2+(j/W)^2+(k/H)^2]}(-1)^{\frac{i+j+k-3}{2}}. \tag{12}$$

The source term C in Eq. (12) is dependent on the reaction rate, the length scale of the body and the permeability, κ; W, and H, which are defined in terms of the permeability in different directions, κ_x, κ_y, and κ_z, are the effective dimensionless width and height of the body:

$$W=\sqrt{\frac{\kappa_x}{\kappa_y}}\frac{L_y}{L_x},\quad H=\sqrt{\frac{\kappa_x}{\kappa_z}}\frac{L_z}{L_x}. \tag{13}$$

After determining the pressure distribution from Eq. (11), we compute the three components of the body forces appearing in Eqs. (6)–(8) as

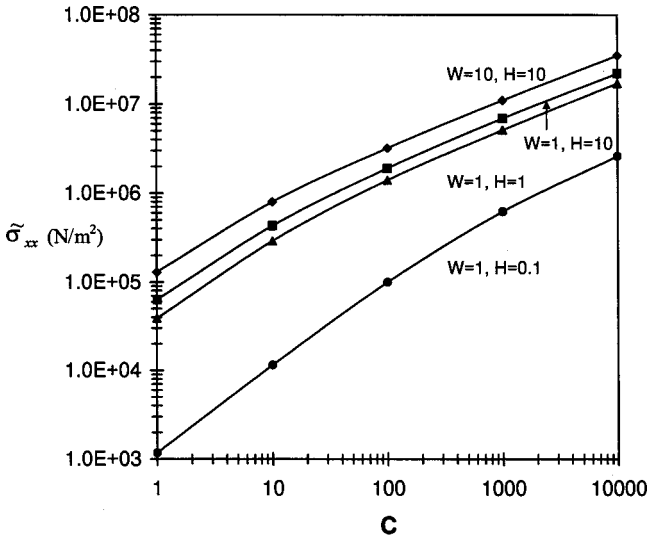

Fig. 2 The dependence of the maximum stress $\tilde{\sigma}_{xx}$ with *C* for parallelipiped bodies of different *W* and *H* with isotropic permeability

$$f_x = -\varepsilon \frac{\partial p}{\partial x}, \quad f_y = -\varepsilon \frac{\partial p}{\partial y}, \quad f_z = -\varepsilon \frac{\partial p}{\partial z}. \tag{14}$$

These body forces are then distributed equally among all nodes in a commercial finite element analysis program, Algor. For "brick" elements in Algor, the body forces of each element are thus equally distributed among the eight nodes in each element. For stress calculations in a rectangular parallelepiped with overall dimensions 2 cm×4 cm×1 cm, we use 125 "brick" elements to represent one-eighth of the body. The product of the void fraction and ambient pressure is taken as $\varepsilon P_0 = 10^5$ N/m^2; because of the linear elasticity assumption, the stresses are proportional to P_0. The void fraction, ε, is therefore left to be arbitrary, and the stresses that are calculated by finite element analysis are thus the nominal stresses which are $(1-\varepsilon)$ times the true stresses on the skeleton. The nominal stresses presented here are due to the pressure gradient alone. For the skeleton material, we use the same material properties as Tsai [15]: $\lambda = 116.8\times10^5$ N/m^2 and $G = 77.9\times10^5$ N/m^2 which corresponds to Poisson's ratio $\nu = 0.3$ and Young's modulus $E = 2\times10^7$ N/m^2.

The stress components $\tilde{\sigma}_{xx}$, $\tilde{\sigma}_{yy}$, $\tilde{\sigma}_{zz}$, and $\tilde{\sigma}_{xy}$ are calculated for a rectangular parallelepiped of overall dimensions of 2 cm×4 cm×1 cm for C=100 with equal permeability ($W=2$, $H=0.5$) in all directions. The maximum pressure in the center of the body is 3.55×10^5 N/m^2 as determined by Eq. (11). Corresponding to this pressure, we find that the maximum normal stresses $\tilde{\sigma}_{xx}$, $\tilde{\sigma}_{yy}$, and $\tilde{\sigma}_{zz}$ are 8.5×10^5 N/m^2, 8×10^5 N/m^2, and 9.9×10^5 N/m^2, respectively, and these maxima all occur at the center of the body as well. The three components of normal stress all decrease monotonically in a nonlinear manner as the edges of the body are approached. The occurrence of the maximum stress in the center of the body agrees with the commonly observed failure mode in that the ceramic parts fracture along surfaces of symmetry corresponding to the normal stresses in the *x* and *y*-directions.

For the case treated above, the maximum shear stresses $\tilde{\sigma}_{xy}$, $\tilde{\sigma}_{yz}$, and $\tilde{\sigma}_{xz}$ are 0.33×10^5 N/m^2, 0.39×10^5 N/m^2, and 0.50×10^5 N/m^2, respectively, and do not occur at the center of the body. We note, in particular, that the maximum shear stresses are at least an order of magnitude smaller than the maximum normal stresses. Calculations on rectangular parallelepipeds with other aspect ratios lead to the same general observation. For this reason, our computational results will be given primarily in terms of the three normal stress components $\tilde{\sigma}_{xx}$, $\tilde{\sigma}_{yy}$, and $\tilde{\sigma}_{zz}$.

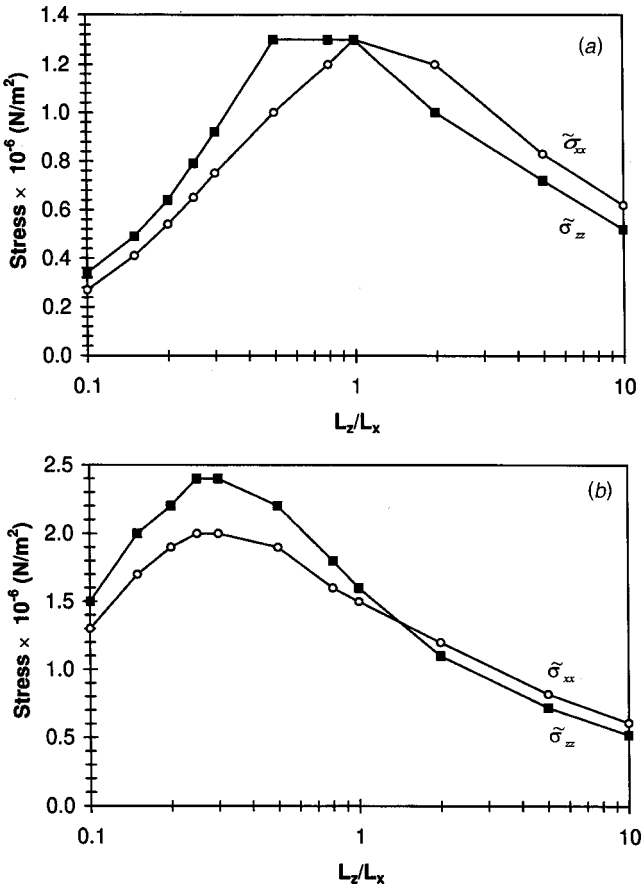

Fig. 3 The dependence of the maximum stresses $\tilde{\sigma}_{xx}$ and $\tilde{\sigma}_{zz}$ with aspect ratio for a square parallepiped body of fixed volume $V=8$ cm^3 with (*a*) equal permeability of $\kappa_x=\kappa_y=\kappa_z=10^{-15}$ m^2 and (*b*) unequal permeability of $\kappa_x=\kappa_y=10^{-15}$, $\kappa_z=10^{-16}$ m^2

Equations (11) and (12) describe the dependence of the pressure distribution on the constant *C*, which is related to the rate of reaction of binder decomposition, the length scale, and the permeability. As a result of Eqs. (6)–(8), the stresses are also dependent on *C*. Figure 2 shows that the maximum normal stress $\tilde{\sigma}_{xx}$ increases with *C* for bodies of isotropic permeability for different values of *W* and *H*. In our previous work [20], we have found that the maximum internal pressure is mainly controlled by the flow of decomposition products across the smallest length of the body; the differences in pressure for the top three cases listed in Fig. 2 are small since the shortest length of these cases is the same. We see from Fig. 2 that this limiting behavior is true for the maximum normal stress $\tilde{\sigma}_{xx}$ as well.

In order to investigate the differences in maximum stress in bodies with anisotropic permeability, we have examined the following two cases: (a) $\kappa_x=\kappa_y=\kappa_z=10^{-15}$ m^2 and (b) $\kappa_x=\kappa_y=10^{-15}$, $\kappa_z=10^{-16}$ m^2. The normal stresses are calculated for bodies of identical volume, $V=8$ cm^3 with $L_x=L_y$, and $L_z=8$ cm$^3/L_x^2$. We also let $C=25$ cm$^{-2}L_x^2$ to correctly account for its dependence on the length scale ([20]). Figures 3(*a*) and 3(*b*) show the maximum normal stresses, and since $\tilde{\sigma}_{xx}=\tilde{\sigma}_{yy}$ for square parallelepipeds, only $\tilde{\sigma}_{xx}$ and $\tilde{\sigma}_{zz}$ are shown. From Fig. 3, we see that in each case, the difference between the two normal stress components is small. In case (a), the maximum normal stress occurs at $L_z/L_x=1$, i.e., the body with cubic geometry. In case (b), the maximum normal stress occurs at L_z/L_x near 0.3. When the different permeability is taken into account in calculating the "effective" aspect ratio *H* by Eq. (12), however, we find

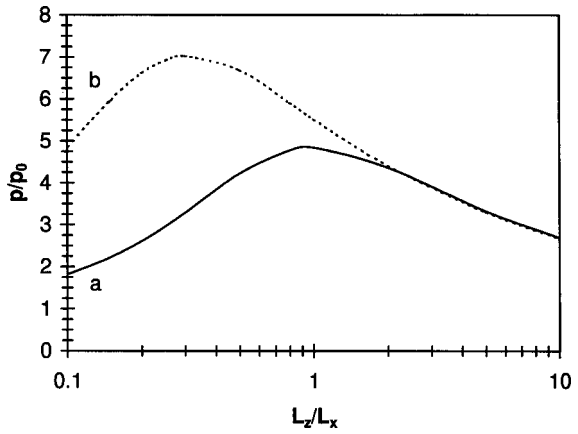

Fig. 4 The dependence of the maximum internal pressure with aspect ratio for a square parallepiped body of fixed volume $V = 8\ \text{cm}^3$ with (*a*) equal permeability of $\kappa_x = \kappa_y = \kappa_z = 10^{-15}\ \text{m}^2$ and (*b*) unequal permeability of $\kappa_x = \kappa_y = 10^{-15}$, $\kappa_z = 10^{-16}\ \text{m}^2$

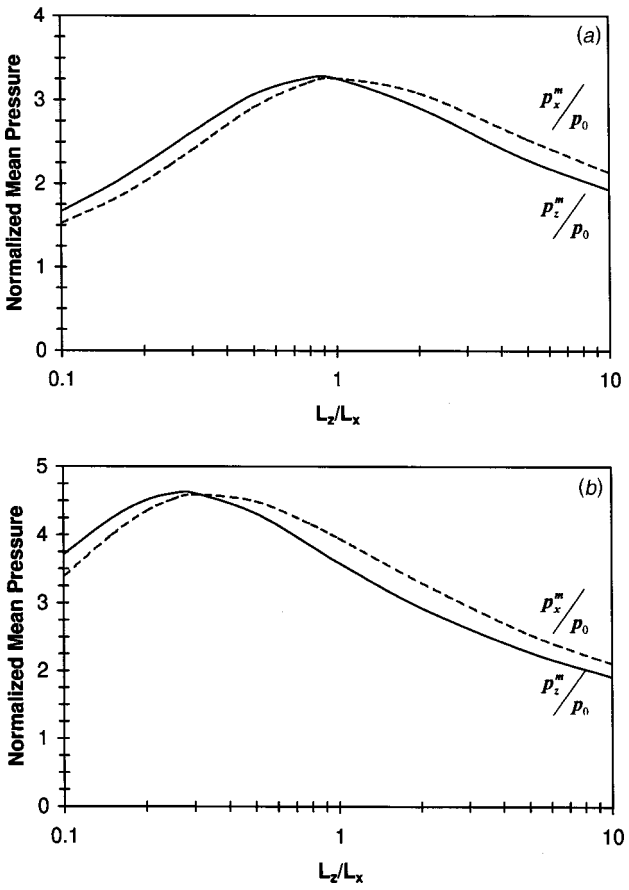

Fig. 5 The dependence of the maximum mean pressure with aspect ratio for a square parallepiped body of fixed volume $V = 8\ \text{cm}^3$ with (*a*) equal permeability of $\kappa_x = \kappa_y = \kappa_z = 10^{-15}\ \text{m}^2$ and (*b*) unequal permeability of $\kappa_x = \kappa_y = 10^{-15}$, $\kappa_z = 10^{-16}\ \text{m}^2$

that the maximum normal stress occurs at $H = 1$. The fact that the stresses vary with L_z/L_x should not be surprising since we are considering parallelepipeds with fixed volume; bodies with either small or large aspect ratios will have one short length scale by which the pressure is relieved, thereby lowering the stress.

The maximum internal pressure corresponding to cases (a) and (b) are shown in Fig. 4. We see that maximum pressure varies with aspect ratio in manner which is very similar to how the stresses in Fig. 3 vary with aspect ratio and permeability. Note especially that the maximum internal pressure occurs at L_z/L_x near 0.3 ($H = 1$) for the case of anisotropic permeability.

The normal stresses shown in Fig. 3(*a*) indicate that $\tilde{\sigma}_{zz}$ is greater than $\tilde{\sigma}_{xx}$ for $L_z < L_x$ and this ordering is reversed for $L_z > L_x$. In other words, the normal stress corresponding to the shorter length is larger than the normal stress corresponding to the longer length. To understand this particular ordering of the normal stresses, we calculate on the three symmetric planes of the body the mean pressures, which are defined as

$$p_x^m = \frac{4}{L_y L_z} \int_0^{L_y/2} \int_0^{L_z/2} p(x=0,y,z)\,dy\,dz \tag{15}$$

$$p_y^m = \frac{4}{L_x L_z} \int_0^{L_x/2} \int_0^{L_z/2} p(x,y=0,z)\,dx\,dz \tag{16}$$

$$p_z^m = \frac{4}{L_x L_y} \int_0^{L_x/2} \int_0^{L_y/2} p(x,y,z=0)\,dx\,dy. \tag{17}$$

Figure 5(*a*) corresponds to case (a) of isotropic permeability, where we see that the ordering of the mean pressures is the same as that of the normal stresses. Thus, for bodies of isotropic permeability, the maximum normal stress and mean pressure both act along the shortest direction.

For case (b) of anisotropic permeability, the mean pressures are plotted in Fig. 5(*b*), where we see that the two curves cross each other at L_z/L_x near 0.3 ($H = 1$). That is, the maximum mean pressure occurs along the shortest direction if the lengths are adjusted by the permeability following Eq. (13). Comparing Fig. 5(*b*) with Fig. 3(*b*), we find that the same cannot be said about the normal stresses; the two curves in Fig. 3(*b*) cross each other when L_z/L_x is near one. In summary, the maximum normal stress and maximum mean pressure occur where the effective aspect ratio H is unity; the aspect ratio at which the ordering of the stress changes, however, occurs at the true aspect ratio L_z/L_x of unity.

Conclusions

We have developed a mechanics model that allows us to calculate the stress distribution in porous three-dimensional bodies based on a known internal pressure distribution. This model, when combined with finite element analysis, allows us to study the stress distribution in ceramic components during binder burnout. This combined approach thus allows one to design bodies based on consideration of the effect of mechanical stresses on product yield.

For the simple geometry we have considered, the normal stresses, which occur at the center of the body, are an order of magnitude larger than the shear stresses. In general, the normal stresses follow the same trends as the internal pressure. This is especially so for bodies with isotropic permeability. Therefore, instead of carrying out stress calculations, which require numerical solution, the internal pressure, for which an analytical solution exists, can often be used for development of the binder burnout cycle and for product design.

During the binder burnout process, very little is known about how the material properties such as the Young's modulus and Poisson's ratio vary spatially and temporally. In addition, the failure criteria have not been identified. In light of these limitations, the mean pressure on different material surfaces can be used as a convenient compromise between the full finite element stress calculations and the internal pressure calculations. Although the mean pressure is calculated solely from the internal pressure, it captures the effect that geometry plays on the distribution of the internal load within the body.

Acknowledgment

One of the authors has benefited greatly from the discussions with Prof. Rohan Abeyaratne.

References

[1] Lewis, J. A., 1997, ''Binder Removal From Ceramics,'' Annu. Rev. Mater. Sci., **27**, pp. 147–173.
[2] Spronson, D. W., and Messing, G. L., 1988, ''Organic Binder Removal Processes in Closed Pore Powder-Binder Systems,'' *Ceramic Transactions*, Vol. 1 (*Ceramic Powder Science IIa*), G. L. Messing, E. Fuller, and H. Hausner, eds., Am. Ceram. Soc., Westerville, OH, pp. 528–537.
[3] Barone, M. R., and Ulicny, J. C., 1990, ''Liquid-Phase Transport During Removal of Organic Binders in Injection-Molded Ceramics,'' J. Am. Ceram. Soc., **73**, pp. 3323–3333.
[4] Lewis, J. A., and Cima, M. J., 1990, ''Diffusivities of Dialkyl Phthalates in Plasticized Poly(Vinyl Butyral): Impact on Binder Thermolysis,'' J. Am. Ceram. Soc., **73**, pp. 2702–2707.
[5] Calvert, P., and Cima, M., 1989, ''Theoretical Models for Binder Burnout,'' J. Am. Ceram. Soc., **73**, pp. 575–579.
[6] Cima, M. J., Lewis, J. A., and Devoe, A. D., 1989, ''Binder Distribution in Ceramic Greenware During Thermolysis,'' J. Am. Ceram. Soc., **72**, pp. 1192–1199.
[7] Evans, J. R. G., Edirisinghe, M. J., Wright, J. K., and Crank, J., 1991, ''On the Removal of Organic Vehicle From Moulded Ceramic Bodies,'' Proc. R. Soc. London, Ser. A, **A432**, pp. 321–340.
[8] Matar, S. A., Edirisinghe, M. J., Evans, J. R. G., and Twizell, E. H., 1993, ''Effect of Porosity Development on the Removal of Organic Vehicle from Ceramic or Metal Moldings,'' J. Mater. Res., **8**, pp. 617–625.
[9] Matar, S. A., Edirisinghe, M. J., Evans, J. R. G., Twizell, E. H., and Song, J. H., 1995, ''Modeling the Removal of Organic Vehicle from Ceramic or Metal Moldings: The Effect of Gas Permeation on the Incidence of Defects,'' J. Mater. Sci., **30**, pp. 3805–3810.
[10] Song, J. H., Edirisinghe, M. J., Evans, J. R. G., and Twizell, E. H., 1996, ''Modeling the Effect of Gas Transport on the Formation of Defects During Thermolysis of Powder Moldings,'' J. Mater. Res., **11**, pp. 830–840.
[11] Matar, S. A., Edirisinghe, M. J., Evans, J. R. G., and Twizell, E. H., 1996, ''Diffusion of Degradation Products in Ceramic Moldings During Thermal Pyrolysis: Effect of Geometry,'' J. Am. Ceram. Soc., **79**, pp. 749–755.
[12] German, R. M., 1987, ''Theory of Thermal Debinding,'' Int. J. Powder Metall., **23**, pp. 237–245.
[13] Lograsso, B. K., and German, R. M., 1990, ''Thermal Debinding of Injection Molded Powder Compacts,'' Powder Metallurgy International, **22**, pp. 17–22.
[14] Stangle, G. Y., and Aksay, I. A., 1990, ''Simultaneous Momentum, Heat and Mass Transfer With Chemical Reaction in a Disordered Porous Medium: Application to Binder Removal From A Ceramic Green Body,'' Chem. Eng. Sci., **45**, pp. 1719–1731.
[15] Tsai, D.-S., 1991, ''Pressure Buildup and Internal Stresses During Binder Burnout: Numerical Analysis,'' AIChE J., **37**, pp. 547–554.
[16] Manguin-Fritsch, A., Burlet, H., Fourt P. M., and Abouaf, M., 1992, ''Modélisation de la Pyrolyse d'un Liant Organique de Mise en Forme de Pièces Céramiques Injectées,'' *L'Industrie Céramique & Verrière*, **887**, pp. 744–749.
[17] West, A. C., and Lombardo, S. J., 1998, ''The Role of Thermal and Transport Properties on the Binder Burnout of Injection Molded Ceramic Components,'' Chem. Eng. J., **71**, pp. 243–252.
[18] Shivashankar, T. S., and German, R. M., 1990, ''Effective Length Scale for Predicting Solvent-Debinding Times of Components Produced by Powder Injection Molding,'' J. Am. Ceram. Soc., **82**, pp. 1146–1152.
[19] Liau, L. C.-K., Peters, B., Krueger, D. S., Gordon, A., Viswanath, D. S., and Lombardo, S. J., 2000, ''The Role of Length Scale on Pressure Increase and Yield of Poly(Vinyl-Butyral)-Barium Titanate-Platinum Multi-Layer Ceramic Capacitors During Binder Burnout,'' J. Am. Ceram. Soc., **83**, pp. 2645–2653.
[20] Lombardo, S. J., and Feng, Z. C., 2002, ''A Model for the Pressure Distribution During Binder Burnout in Three-Dimensional Porous Ceramic Bodies With Anisotropic Permeability,'' J. Mater. Res., accepted for publication.
[21] Peters, B., and Lombardo, S. J., 2001, ''Optimization of Multi-Layer Ceramic Capacitor Geometry for Maximum Yield During Binder Burnout,'' J. Mater. Sci., **12**, pp. 403–409.
[22] McTigue, D. F., Wilson, R. K., and Nunziato, J. W., 1983, ''An Effective Stress Principle for Partially Saturated Granular Media,'' *Mechanics of Granular Materials: New Models and Constitutive Relations* J. T. Jenkins, and M. Satake, eds., Elsevier, Amsterdam, pp. 195–210.
[23] Coussy, O., 1995, *Mechanics of Porous Continua*, John Wiley and Sons, New York.
[24] Fung, Y. C., 1965, *Foundations of Solid Mechanics*. Prentice-Hall, Englewood Cliffs, NJ.
[25] suggested by a reviewer.
[26] Green, A. E., and Naghdi, P. M., 1965, ''A Dynamical Theory of Interacting Continua,'' Int. J. Eng. Sci., **3**, pp. 231–241.
[27] Ortiz, M., 1985, ''A Constitutive Theory for the Inelastic Behavior of Concrete,'' Mech. Mater., **4**, pp. 67–93.
[28] Harr, M. E., 1997, *Mechanics of Particulate Media*, McGraw-Hill, New York.